

Sea ice, atmosphere and upper ocean variability in the Weddell Sea, Antarctica

Silvia A. Venegas

Danish Center for Earth System Science, Niels Bohr Institute for Astronomy, Physics and Geophysics, University of Copenhagen, Copenhagen, Denmark

Mark R. Drinkwater¹

Oceans/Ice Unit, European Space Agency, Noordwijk, The Netherlands

Abstract. A frequency domain singular value decomposition is performed on 20 years (1979-1998) of monthly sea ice concentration, sea ice drift and sea level pressure data in the Weddell Sea, Antarctica. Interannual oscillations with periods of around 3-4 years are found to dominate the variability in this region. Anomalous atmospheric patterns periodically reach the Weddell Sea from the west and perturb the sea ice circulation and distribution in the Weddell Gyre through changes in the intensity and direction of the climatological winds. Sea ice accumulates in the southeastern Weddell Sea every 3-4 years owing to two atmospherically driven processes: (1) weak ice export to the north due to a weak northward branch of the gyre (driven by weak southerly winds) and (2) large ice import from the east due to a strong East Wind Drift (driven by strong easterly winds along the coast). The opposite situation gives rise to a depletion of sea ice in the same region half a cycle later. Sea ice anomalies are then advected north-northeastward before turning eastward in the gyre circulation. The eastward propagation of ice anomalies along the ice margin accounts for the passage of the Antarctic Circumpolar Wave through the Atlantic sector of the Southern Ocean. A low frequency signal is also detected in the Weddell Sea variations, albeit rather speculatively in this 20-year-long record. Sea ice variability on this timescale appears to be associated with a change in the shape and characteristics of the Weddell Gyre circulation around 1990. This mode of variability implicates feedbacks between the gyre and Weddell Deep Water temperature variations, whose impact is observed near the Maud Rise topographic feature.

1. Introduction

Sea ice around Antarctica modulates the interaction and coupling between the atmosphere and the ocean. A detailed description of the sea ice dynamics and thermodynamics is therefore necessary for understanding the impact of the air-ice-sea exchange upon the Antarctic climate variability. Both thermodynamic and dynamic processes play significant

roles in this variability. Thermodynamics controls the ice growth that rapidly replaces sea ice in open water regions, while dynamics affects the displacement and dislocation of the sea ice thereby limiting the geographic distribution of exposed open water in leads and polynyas. Opening and closing of the sea ice pack in response to variability in ice motion essentially regulate the heat and momentum exchange between ocean and atmosphere.

Under divergent ice conditions, reduced sea ice concentrations enhance air-sea heat fluxes. This allows ice forma-

¹Formerly at Jet Propulsion Laboratory, California Institute of Technology, Pasadena, California, USA.

tion to rapidly replace the open water areas with ice, particularly in winter. The brine rejection process, which accelerates under vigorous growth, acts to destabilize the upper water column [Martinson and Iannuzzi, 1998]. Negative buoyancy imparted by brine rejection causes overturning and thus more heat to be delivered to the surface to be vented to the atmosphere. Such convective or upwelling conditions around Antarctica can lead to large quantities of heat released to the atmosphere but require persistent ice divergence to remain active. Typically, such bursts of heat flux are shut off by ice convergence and by the same heat causing melting of the sea ice and a restabilization of the mixed layer. Only one polynya event has been recorded in the satellite era during which convection persisted throughout several seasons [Gordon and Comiso, 1988; Comiso and Gordon, 1996].

A contrasting set of mechanisms occur during convergent ice conditions. Dynamic thickening of sea ice by ridging and rafting is the main process by which ice becomes thicker around Antarctica, since the effect of thermodynamic ice growth is relatively limited. Convergent conditions are typically brought about by persistent ice drift toward the coast of Antarctica. Thickening of the ice reduces the conductive heat flux through the ice and switches off the heat conduction between the atmosphere and the ocean [Maykut, 1978]. During such conditions, the increased roughness of the ice surface enhances the momentum transfer via air-ice drag [Martinson and Wamsler, 1990; Fisher and Lytle, 1998], and in doing so allows a more rapid advection of the sea ice.

Seasonal and interannual variability of the sea ice cover has a significant impact on water mass modification processes, particularly in the Weddell and Ross Sea basins [Jacobs and Comiso, 1989; Comiso and Gordon, 1998; Markus *et al.*, 1998]. In these two key regions, ice formation and melting influence the upper ocean stability by changing the salinity and buoyancy gradients [Martinson and Iannuzzi, 1998]. Both mechanisms may have an impact upon the water mass modification processes driving the global thermohaline circulation.

Previous experimental studies in the Weddell Sea, such as the Ice Station Weddell [Gordon *et al.*, 1993] and the Antarctic Zone Flux Experiment (Anzflux) [McPhee *et al.*, 1996] have focused on processes and couplings on subdaily to seasonal timescales. This work takes a larger perspective, choosing instead to focus in detail upon the links between the sea ice, the upper ocean, and the atmospheric fluctuations in the Weddell Sea basin on interannual and longer timescales. White and Peterson [1996] presented a heuristic global framework for coupled oscillations in the Southern Ocean, with persistent, propagating coupled sea surface temperature, sea level pressure, and ice extent anomalies. Yuan *et al.* [1999] recently demonstrated that the sea ice mar-

gin does not simply respond passively to atmospheric forcing, but that changes in its spatial configuration in response to synoptic low-pressure systems can lead to enhanced sea level pressure and thermal gradients which in turn can provide conditions favorable to cyclogenesis. Here we choose to focus on the entire coupled regional system in the Weddell Sea. A sequence of coupled dynamic and thermodynamic processes taking place between ocean, ice, and atmosphere is proposed to account for the observed variability.

A brief description of the data and methodology used is given in section 2. The Weddell Sea climatology and the dominant timescales of ice and atmospheric variability are described in section 3. The quasi-quadrennial and long-term signals detected are analyzed in detail in sections 4 and 5, respectively. The temporal characteristics of both sea ice signals are briefly described in section 6. Finally, section 7 presents a short discussion and conclusions.

2. Data and Method

The data used in this work consist of monthly means of sea ice concentration, sea ice drift (zonal and meridional components), and sea level pressure in the Weddell Sea region, i.e., from 90°W to 60°E and from 55°S to the South Pole. The records span a 20-year period, extending from January 1979 to December 1998, except for the ice drift data, for which only 19 years are available (to December 1997). Monthly anomalies are constructed by subtracting the 20-year climatological monthly means from the original data.

Sea ice concentration (SIC) data were derived from a combination of Nimbus 7 Scanning Multichannel Microwave Radiometer (SMMR) and Special Sensor Microwave/Imager (SSM/I) satellite passive microwave observations. These data started with the launch of Nimbus 7 in 1978 and continued with the SSM/I series beginning in 1987 [Cavalieri *et al.*, 1997a, 1999]. The SIC data sets were processed and provided by the EOS Distributed Active Archive Center (DAAC) at the National Snow and Ice Data Center (NSIDC) [National Snow and Ice Data Center, 1995]. Ice concentrations are gridded at a spatial resolution of 25 × 25 km, and their values represent the fraction of the grid area covered by sea ice. Ice concentration values range from 0 (for no sea ice in the grid area) to 1 (for a completely ice-covered grid area).

The ice drift (ID) data are a gridded, optimally interpolated data set derived from a combination of satellite and buoy tracking. Satellite ice drift estimates were made by computer tracking of features in 6 times oversampled SSM/I passive microwave brightness temperature images (at 85 and 37 GHz) spaced at intervals of 2 days, using a previously described technique [Kwok *et al.*, 1998; Drinkwater *et al.*,

1999a]. Satellite ice motion tracking techniques matured significantly over the last several years, and similar ice results have been reported elsewhere [Agnew *et al.*, 1997; Emery *et al.*, 1997; Maslanik *et al.*, 1998; Martin and Augstein, 2000]. Comparisons between buoy and 2-day satellite ice drift data indicate a Gaussian zero-mean error distribution with a displacement standard deviation of the order of 5 km or less in 2-day drift, or ~ 4 cm/s [Maslanik *et al.*, 1998]. In this ID data set, satellite ice motion estimates were combined with Weddell Sea buoy data from the International Programme for Antarctic Buoys using an optimal interpolation scheme similar to that proposed by Drinkwater *et al.* [1999b] and reported by Kwok [2000]. The ice drift estimates were objectively analyzed (with higher weightings applied to the buoy data set) to generate an optimally interpolated ID product. The advantage of this procedure is a gap-filled gridded motion vector field that takes advantage of in situ buoy data where and when available. We have subsequently generated monthly averages of the gridded ID data. Since Weddell Sea ice drift decorrelates on timescales typically of less than 1 day [Drinkwater, 1998a], bidaily samples of ice drift are assumed to be independent. If according to Kwok *et al.* [1998] satellite tracking uncertainties are considered unbiased additive noise, then averaging reduces the noise contribution to the estimates of mean drift in proportion to $1/\sqrt{N}$, where $N \sim 15$ is the number of observations averaged per month. Monthly averages reduce the standard error of the mean x and y component drift speeds by a factor of 4 to less than 1 cm/s.

The sea level pressure (SLP) data are obtained from the National Center for Atmospheric Research/National Centers for Environmental Prediction (NCAR/NCEP) Reanalysis Project [Kalnay *et al.*, 1996]. They have a spatial resolution of $2.5^\circ \times 2.5^\circ$ and are classified under the reanalysis class A. This indicates that they are strongly influenced by observed data and little influenced by the model predictions; i.e., they belong to the most reliable type of reanalysis data.

Time series of air-sea latent plus sensible turbulent heat flux data are also obtained from the NCAR/NCEP Reanalysis Project and have a spatial resolution of $2.5^\circ \times 2.5^\circ$. They are classified as class C; that is, they are strongly influenced by the model predictions, in particular in the high southern latitudes involved in this work. We are aware of this fact when drawing conclusions from the heat flux analyses.

Here we apply the multitaper method-singular value decomposition (MTM-SVD), a multivariate signal detection technique developed by Mann and Park [1999]. With this method we seek to identify statistically significant narrow-band oscillations that are correlated among a large number of time series (gridded data points). A brief summary of the procedure is given below. For details and an extensive de-

scription of this technique, the reader is referred to Mann and Park [1999]. Recent climate applications can be found in the work of Mann and Park [1994, 1996], Tourre *et al.* [1999], and Venegas and Mysak [2000].

Each grid point time series is first transformed from the time to the spectral domain using the MTM approach for spectral estimation. The MTM method applies a number (K) of orthogonal windows (tapers) to the data, in order to calculate power spectrum estimates with an optimal trade-off between spectral resolution and variance [Thomson, 1982; Percival and Walden, 1993]. In our analysis, $K = 3$ independent spectral estimates are computed for each of the M time series by multiplying them by a family of three orthogonal data tapers ($Y_k^m(f)$; tapers $k = 1, 2, 3$; grid points $m = 1, \dots, M$; frequency f). At each frequency, the three spectral estimates for the M time series are organized in the following $M \times 3$ matrix:

$$\mathbf{A}(f) = \begin{bmatrix} Y_1^1(f) & Y_2^1(f) & Y_3^1(f) \\ Y_1^2(f) & Y_2^2(f) & Y_3^2(f) \\ \vdots & \vdots & \vdots \\ Y_1^M(f) & Y_2^M(f) & Y_3^M(f) \end{bmatrix}.$$

A singular value decomposition is then performed on each matrix $\mathbf{A}(f)$. At a given frequency, the first singular value of the decomposition is proportional to the variance accounted for by the most significant signal detected in the data within a narrow band around that frequency. A local fractional variance (LFV) spectrum is then constructed by plotting the percentage of variance explained by the first mode at each frequency. After performing a test of statistical significance through a bootstrap resampling technique [Efron, 1990; Mann and Park, 1999], the dominant timescales of variability in the data can be identified as the frequencies showing the largest significant peaks in the LFV spectrum. The first spatial and spectral empirical orthogonal functions (EOF) of the singular value decomposition are then used to reconstruct the anomaly spatial patterns and temporal evolution associated with the selected significant frequencies (see Mann and Park [1999] for further details on the anomaly reconstruction). A ‘‘joint’’ MTM-SVD analysis between the three variables SIC, ID, and SLP is also performed here by applying the described technique to an aggregate data matrix that includes the three fields one after the other (that is, rows $m = 1, \dots, N$ for SIC; rows $m = N+1, \dots, L$ for ID; and rows $m = L+1, \dots, M$ for SLP). This joint analysis identifies the dominant timescales of variability on which the three fields exhibit significant coherence.

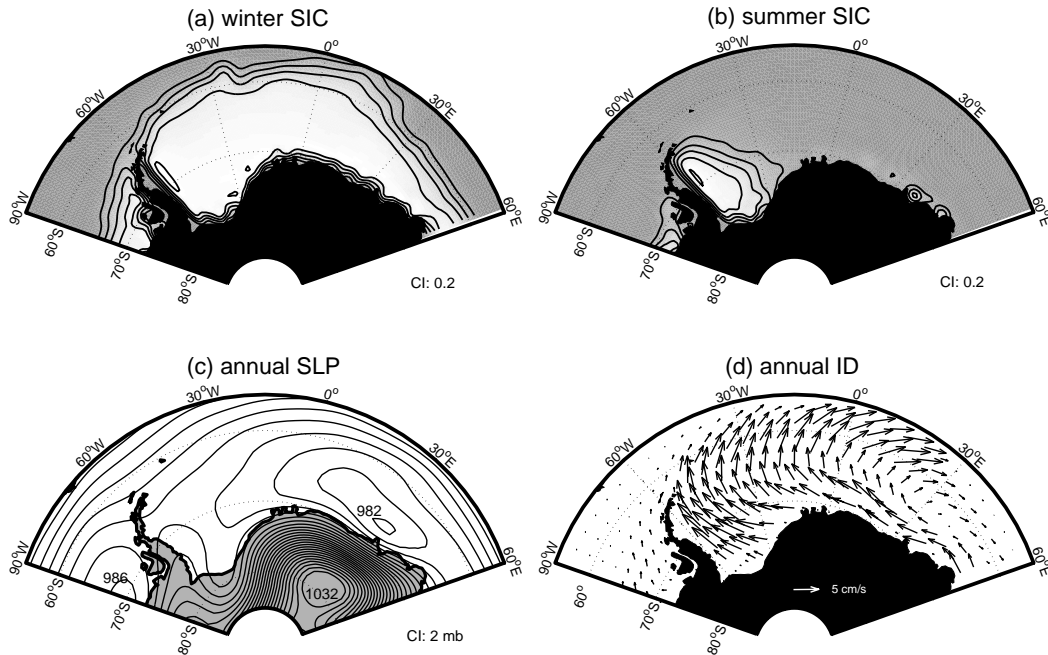


Figure 1. The 20-year climatology 1979-1998 for the (a) winter sea ice concentration (June-September), (b) summer sea ice concentration (December-March), (c) annual sea level pressure, and (d) annual ice drift fields in the Weddell Sea. The ice drift field is shown for the case of maximum (winter) sea ice extent. CI, contour interval.

3. Climatology and Dominant Timescales of Variability

Figure 1 shows the 20-year climatologies 1979-1998 for the winter SIC (June-September), summer SIC (December-March), and annual SLP and ID fields in the Weddell Sea basin. During the winter (Figure 1a), the sea ice cover attains its maximum northward extent, reaching latitudes of around 55° - 60° S. During the summer (Figure 1b), most of the winter sea ice melts, and only a narrow region along the Antarctic Peninsula remains ice covered the year round (perennial ice).

The SLP annual climatology (Figure 1c) shows a zonally elongated low-pressure belt along and off the coast of Antarctica (the Circumpolar Trough [Harangozo, 1997]) and a strong high-pressure center over the continent. The low-pressure belt is broken near 50° W by a high-pressure ridge extending northward from the continent over the Antarctic Peninsula. The ID climatology (Figure 1d) clearly shows the Weddell Gyre as sea ice circulating cyclonically around the basin. The sea ice motion is basically driven by the SLP configuration through a relationship with the geostrophic

wind [Thorndike and Colony, 1982; Kottmeier and Sellmann, 1996; Drinkwater, 1998a] and on the average drifts parallel to the isobars. The Weddell Gyre, which in this case is traced out by the ice drift [Deacon, 1984; Emery *et al.*, 1997], is composed of a narrow westward branch flowing along the Antarctic coast, called the East Wind Drift, a northward branch along the Antarctic Peninsula, and a wide eastward drift along the winter ice edge following the Antarctic Circumpolar Current.

The LfV spectrum obtained from the application of the MTM-SVD method to the joint monthly SIC, SLP, and ID anomalies is shown in Figure 2a and reveals the timescales on which the three variables exhibit coherent variability. A statistically significant signal is identified in the broad frequency band between 0.25 and 0.33 cycle yr^{-1} , that is, periods of about 3-4 years. This signal also stands out as significant in each of the three individual spectra shown in Figure 2b. Ice and atmospheric oscillations on this timescale are consistent with the Antarctic Circumpolar Wave (ACW [White and Peterson, 1996; Jacobs and Mitchell, 1996]). The broadness of the peak indicates frequency modulation during the 20 years. We will refer to this variability as the

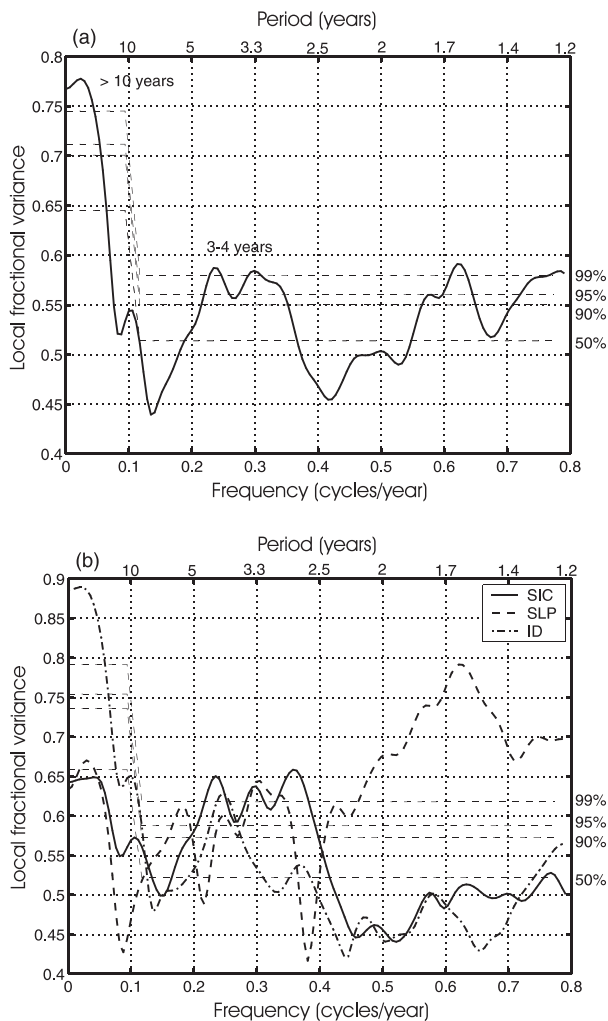


Figure 2. (a) Local fractional variance (LFV) spectrum of the joint SIC, SLP, and ID anomalies based on the 20-year period 1979-1998, with significance levels obtained from bootstrap resampling. A broad significant peak stands out in the quasi-quadrennial band (periods of about 3-4 years). A very low frequency signal, not resolved from a trend in a 20-year record, is also significant. (b) LFV spectra of the three variables analyzed separately. The significance levels shown are those calculated for the SIC anomalies. The SLP and ID spectra are renormalized so that the significance levels also apply to them.

quasi-quadrennial signal in the Weddell Sea. It will be further analyzed in section 4.

In addition to the interannual peak, a very low frequency signal with period longer than 10 years (frequencies smaller than $0.1 \text{ cycle yr}^{-1}$) stands out as significant in Figure 2a

and is very intriguing. The shortness of the available data record does not allow for a more precise determination of its period, hence this signal may either be a long-term trend or a decadal-scale fluctuation with period longer than 10 years. The signal is also significant in the ice drift independent spectrum shown in Figure 2b, which indicates the dominance of this variable over the other two in driving the variability on this timescale. Section 5 provides a closer examination of this long-term signal.

Finally, a third significant peak is detected in Figure 2a at around $0.6 \text{ cycle yr}^{-1}$ (biennial timescale). This high-frequency peak appears in the joint analysis only owing to the influence of the SLP data, since this timescale is not significant in the ice spectra of Figure 2b. Therefore, this atmospheric signal will not be further considered in this study.

A similar analysis is performed on the seasonally averaged SIC anomalies for the periods January-March, April-June, July-September, October-December (not shown). The quasi-quadrennial signal is found to be equally significant in the four seasons. The long-term trend, however, is only significant during summer and fall. This may suggest a large-scale connection with Arctic sea ice and atmosphere decadal-scale signals, which are strongest during the Northern Hemisphere winter [Venegas and Mysak, 2000].

4. The Quasi-Quadrennial Signal

Plates 1 and 2 show the first and second half, respectively, of an average quasi-quadrennial cycle. The cycle is divided into eight equally spaced snapshots in order to observe the temporal evolution of the anomalies during consecutive phases.

The SIC anomalies seem to propagate clockwise following the gyre circulation around the Weddell basin during a cycle. Two main centers of action are observed: one in the southeastern Weddell Sea off Coats Land and the Riiser-Larsen Ice Shelf and the other in the northern Weddell Sea, in the vicinity of South Orkney Island spreading from the tip of the Antarctic Peninsula toward the east along the winter ice margin. We will call these SIC features the “Coats Land (CL) anomaly” and the “South Orkney (SO) anomaly.”

It is important to note that the spatial patterns in Plates 1 and 2 show the “average” anomalies during a cycle. Although separated by 6-month intervals, the different snapshots do not necessarily represent the alternating seasons of each consecutive year, but rather an average picture of all seasons. The method identifies grid points where significant ice concentration anomalies do occur, without distinguishing whether they occur simultaneously or not. In the case of the SIC data, this is an important issue, since the ice margin (along which SIC anomalies are seen) changes position with

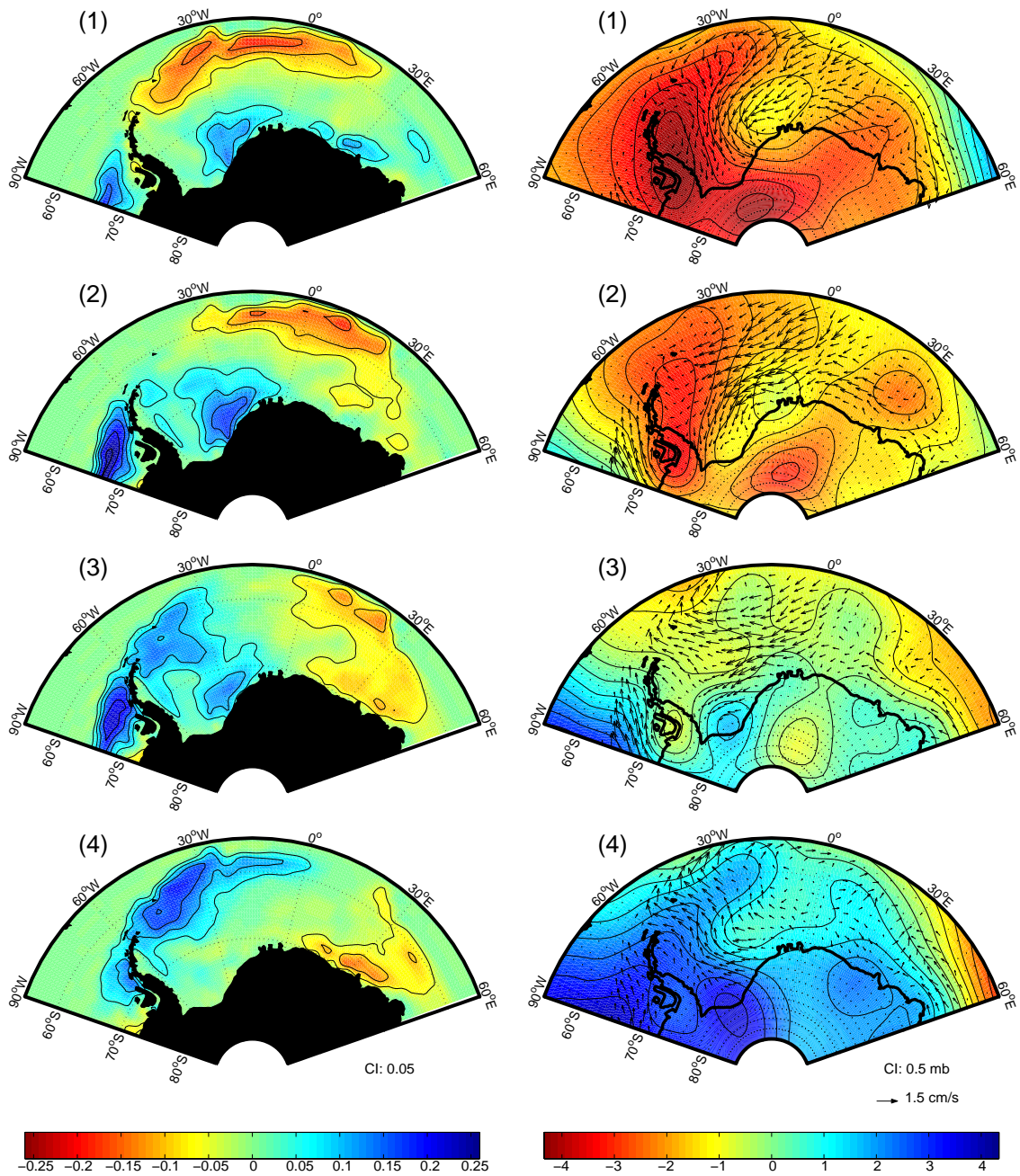


Plate 1. Spatial reconstruction of the monthly (left) SIC anomalies and (right) SLP and ID anomalies during the first half of an average quasi-quadrennial cycle. The patterns are shown at four consecutive snapshots separated by approximately 6 months. The ID patterns are shown for the case of maximum (winter) sea ice extent. Numbers 1-4 correspond to snapshots 1-4. Zero contour is omitted in the SIC patterns. CI, contour interval.

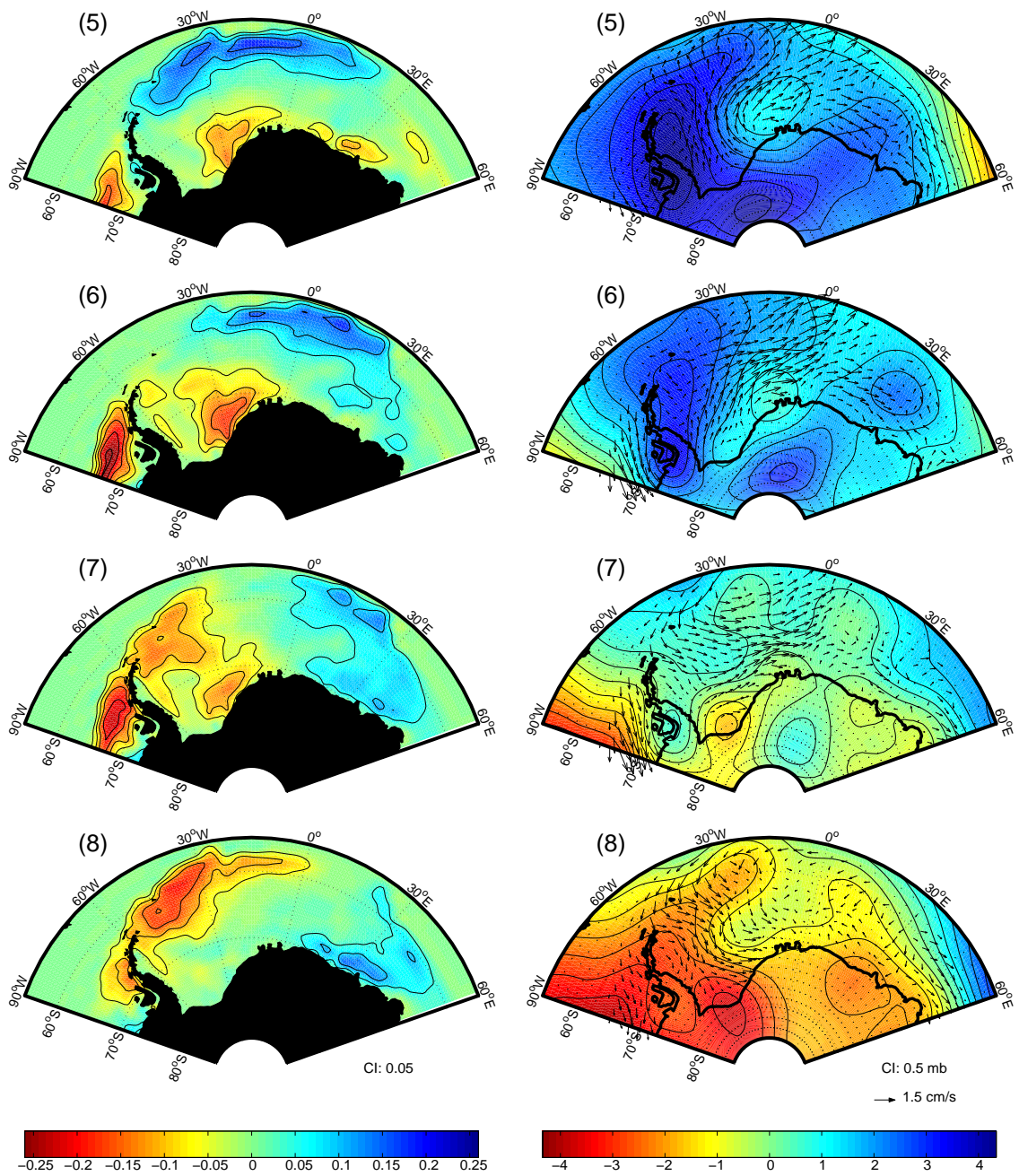


Plate 2. Spatial reconstruction of the monthly (left) SIC anomalies and (right) SLP and ID anomalies during the second half of an average quasi-quadrennial cycle. Numbers 5-8 correspond to snapshots 5-8. Conventions as in Figure 1

the seasons. As such, even though the two SIC centers appear at the same time in these average patterns, they cannot in reality be “seen” simultaneously. The CL anomaly is only manifested in the SIC data during the summer-fall months as an anomalous extension of the summer ice cover (see Figure 1b). It cannot be detected in the SIC data during winter, when the southern Weddell Sea is completely ice covered and all SIC values are equal to 1. However, it remains in the form of an ice thickness anomaly, which the satellite cannot detect. Similarly, the SO anomaly can only be seen in the SIC data during the winter-spring months, when the ice cover reaches its maximum extent (see Figure 1a). When the ice melts and retreats in summer, however, an upper ocean freshwater anomaly likely remains in its place.

The SLP anomalies in snapshots 1-2 and 5-6 (Plates 1 and 2) exhibit a center of anomalous low/high pressure over the Antarctic Peninsula that extends northeastward up to around 30°W-60°S. This anomalous atmospheric pattern disturbs the wind-driven ID in the Weddell Gyre through changes in the intensity and direction of the climatological mean winds. ID patterns are shown superimposed onto the winter (maximum) ice cover to better appreciate the drift patterns that drive the SIC anomalies. They are similar during other seasons but are spatially limited to the area where ice is present in each season.

4.1. The Coats Land Anomaly

The anomalous SLP pattern in snapshots 1-2 (5-6) reduces (strengthens) the SLP gradient between the climatological low pressure in the Circumpolar Trough and the ridge of high pressure over the Antarctic Peninsula shown in Figure 1c. The climatological southerly winds parallel to the Antarctic Peninsula are reduced (enhanced), thereby driving a weak (strong) ID in the northward branch of the gyre and reducing (enhancing) the export of ice from the Weddell basin to the north. On the other hand, the climatological East Wind Drift is reinforced (opposed) by westward ID anomalies along the coast, which results in enhanced (reduced) inflow of ice into the Weddell basin from the east. The combined effect of a reduced (enhanced) ice export to the north and enhanced (reduced) ice import from the east results in convergence (divergence) of ice in the inner Weddell Sea. This process is reflected by the positive (negative) CL anomaly in steps 1-2 (5-6). Time series in Figure 3a illustrate how a weak (strong) zonal SLP gradient to the east of the Antarctic Peninsula leads the formation of a positive (negative) CL anomaly by 6-8 months.

Ice accumulating in the CL region in steps 1-2 deforms by ridging/rafting and by compression of new ice periodically formed in coastal polynyas. The latter process was clearly observed in this region during the Winter Weddell

Gyre Study in 1992 [Lemke, 1994; Drinkwater, 1998a]. The meridional winds changed direction with a significantly stronger component of onshore flow, and the German research vessel *Polarstern* was beset by ice due to severe ice pressure against the coast in the Kapp Norvegia region (Akta Bay). Associated with the anomalous wind distribution in 1992 was the development of an area of particularly deformed, compressed sea ice along the Antarctic coast from 5°W to 20°W. In situ helicopter-borne laser profiling of the sea ice surface [Dierking, 1995], together with upward looking sonar data [Harms *et al.*, 2001] in this region, confirm the origin and formation of ice thickness anomalies upstream of the CL region. This process is identified by Drinkwater *et al.* [2001] as being responsible for significant interannual variations in volumetric import of sea ice along the CL coast, together with the large seasonal peak observed in winter 1992. The positive CL SIC anomaly in snapshots 1-2 is an indication of ice accumulating from such an atmospherically driven process.

Although the CL SIC anomaly of steps 1-2 can only be detected in summer, an ice thickness anomaly presumably remains in the region during the subsequent winter, since deformation and compression of ice imply thickening of the ice layer. Ice deformation develops ridge sails, and as the ice surface roughens, the form drag increases [Banke *et al.*, 1980; Martinson and Wamser, 1990; Fisher and Lytle, 1998], thereby increasing momentum transfer to the ice. This feeds back into a more effective transport of ice from the east and further deformation. The increased thickness and volume of sea ice in the region reduces the air-sea heat exchange, limiting the interaction between ocean and atmosphere [Maykut, 1978]. Consequently, the upper water column becomes stratified, leading to stable upper ocean conditions.

The opposite situation occurs in steps 5-6, where divergence of ice in the inner Weddell Sea is also observed along the Ronne and Filchner Ice Shelves as larger-than-normal polynya opening events [Drinkwater, 1998b]. The reduction in the amount of sea ice results in enhanced cooling of the ocean surface layer promoting sea ice formation in the open water areas [Kottmeier and Engelbart, 1992]. Brine rejection due to new ice formation preconditions the upper water column for convective overturning and deep water formation [Gordon and Huber, 1990; Fahrback *et al.*, 1995].

4.2. The South Orkney Anomaly

The CL anomaly stops growing as soon as the SLP pattern changes in snapshots 3-4 (Plate 1) and 7-8 (Plate 2). During the year following its formation, the anomaly is advected northward by the mean gyre circulation. This advection is detected in the SIC data only along the summer-

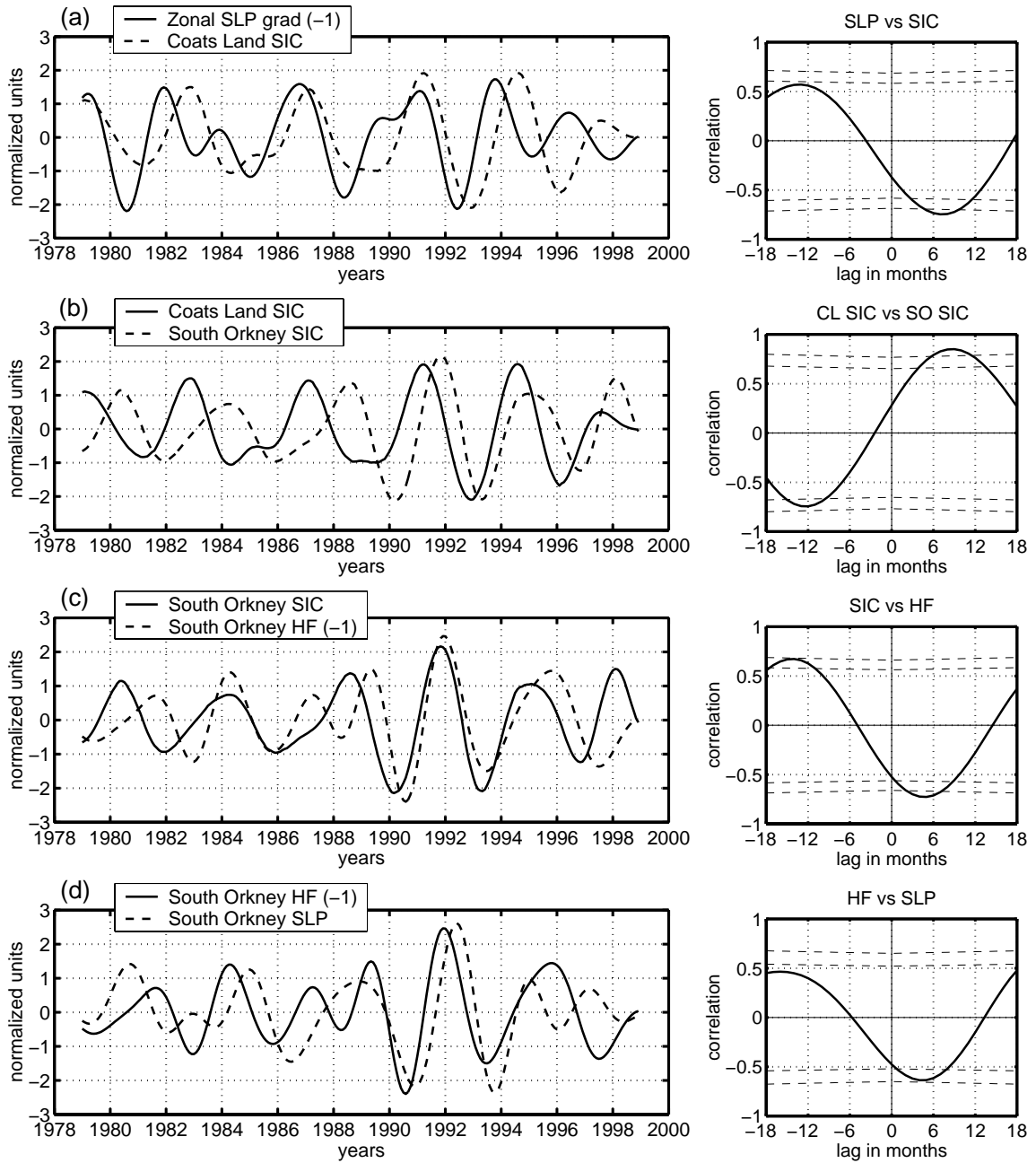


Figure 3. (left) (a) Temporal evolution of the zonal SLP gradient to the east of the Antarctic Peninsula and the CL SIC anomaly. The zonal SLP gradient is defined as the pressure at 60°W - 68°S minus that at 15°W - 68°S (see straight line in Figure 4). The CL SIC anomaly is averaged over the region 45° - 15°W and 65° - 77°S . (b) Temporal evolution of the CL SIC anomaly and the SO SIC anomaly (averaged over the region 60° - 15°W and 55° - 65°S). (c) Temporal evolution of the SO SIC anomaly and the anomalous heat flux to the atmosphere in the SO region (by -1). (d) Temporal evolution of the anomalous heat flux to the atmosphere in the SO region (by -1) and the anomalous SLP over the SO region. All monthly time series are band passed with an admittance window of 2-5 years [Kaylor, 1977] and normalized by the respective standard deviation. (right) Lagged correlation function between the two time series in each panel, with 90% and 95% significance levels (dashed lines). The first quantity leads the second for positive lags.

fall ice margin (snapshots 3 and 7), but it also occurs during winter-spring, when the region is ice covered, in the form of an ice thickness anomaly moving northward. The CL anomaly reaches the northern Weddell Sea the following year and becomes the SO anomaly. There it is further reinforced by strong southerly winds associated with the new SLP pattern (snapshots 4 and 8). Figure 3b illustrates the advection of the SIC anomaly from the CL region toward the SO region by showing the lead-lag relationship between the SIC time series in the two regions. The sea ice needs around 8-10 months to be swept out of the basin from the southern Weddell Sea, which requires typical ice drift velocities of around 6-8 km/d ($\sim 6-8$ cm/s) for the ice to cover this path of about 1800 km. Positive (negative) peaks in the CL time series correspond to snapshot 2 (6). Positive (negative) peaks in the SO time series correspond to snapshot 4 (8).

The SO anomaly is then advected eastward along the ice margin by the Weddell Gyre circulation and the Antarctic Circumpolar Current (snapshots 4-6 and 8-2). Along its way, it is sustained from dissipation by the meridional component of the anomalous winds. These reinforce the positive (negative) ice edge anomaly through two mechanisms: (1) by advection of cold (warm) air which promotes ice formation (melting) and (2) by air-ice drag that forces the ice to drift offshore (onshore), i.e., by expansion (compression) of the ice pack. In addition to the atmospheric forcing, the positive (negative) SO anomaly is also sustained by the positive (negative) freshwater anomaly that accompanies the ice, which stabilizes (destabilizes) the mixed layer thereby decreasing (increasing) the oceanic heat loss to the atmosphere and reducing (enhancing) the melting rate at the ice-edge. This process reinforces the original positive (negative) anomaly, resulting in a positive feedback. To the east of 0° longitude, the wind forcing disappears and the ice edge anomaly begins to weaken. Around 30°E it moves southward following the ice margin, which in this sector of Antarctica is closer to the continent, until it is partly trapped in the East Wind Drift and carried westward along the coast. A weak residual signal continues eastward along the ice margin.

The center of the SO anomaly takes around 1-1.5 years to travel from 45°W to around 10°E along the ice margin, implying an approximate speed of propagation of 6-9 cm/s. This is consistent with the speeds of the ACW estimated from observations by *White and Peterson* [1996] and *Jacobs and Mitchell* [1996] and with mean current speeds in the Antarctic Circumpolar Current simulated by the Fine Resolution Antarctic Model (FRAM [*Ivchenko et al.*, 1999]).

Snapshots 1 and 5 show a SIC anomaly of the same sign as the CL anomaly approaching the western coast of the Antarctic Peninsula from the Bellingshausen Sea. This anomaly reaches the tip of the peninsula from the west

precisely at the same time as the CL anomaly meets it from the south. Actually, there is negligible flux of ice around the tip of the peninsula (S. E. Stammerjohn, University of California, Santa Barbara, personal communication, 2000), and therefore these two ice concentration anomalies are independent and unconnected with one another. They appear to be synchronized, and “in phase” at the tip of the Antarctic Peninsula because they are both essentially driven by the same large-scale anomalous atmospheric pattern (S. A. Venegas, M. R. Drinkwater and G. Shaffer, Coupled oscillations in Antarctic sea ice and atmosphere in the South Pacific sector, submitted to *Geophysical Research Letters*, 2001)(hereinafter Venegas et al., submitted manuscript, 2001). *White and Peterson* [1996] describe these two in-phase ice anomalies as one propagating wave in “northward ice extent” traveling eastward along the ice edge from the Pacific to the Atlantic sectors of Antarctica. Using ice concentration data, we detect the existence of the CL anomaly moving northward and the ice dynamics anomaly which reinforces ice flux at the ice margin. This illustrates some of the coupling required to sustain the ice margin anomalies observed by *White and Peterson* [1996].

4.3. Feedback to the Atmosphere

The presence or absence of sea ice regulates the interaction between ocean and atmosphere. Reduced ice concentration conditions imply large open water areas and a drastic increase of the amount of heat released from the ocean to the atmosphere. Enhanced heat flux to the atmosphere implies destabilization of the upper ocean mixed layer and increased overturning. This brings warm deep water to the surface, allowing more heat to be vented to the atmosphere (a positive feedback). Sea-to-air heat flux produces a relative warm, and thus more buoyant, atmospheric boundary layer over the region of low ice concentration, which is translated into a decrease in atmospheric pressure. Such a response of the atmospheric pressure to reduced ice concentration is well illustrated by the consecutive steps 8-1-2. The presence of the negative SO anomaly implies a retreat of the winter ice edge and enhanced oceanic heat loss. The atmospheric response to the anomalous warming is the development of an elongated SLP trough over the region of reduced ice extent, from the tip of the Antarctic Peninsula to the east. The opposite process occurs in steps 4-5-6. This results in a change of polarity of the SLP pattern over the Weddell Sea. Figure 3c shows how a positive (negative) ice edge anomaly in the SO region leads to weak (strong) oceanic heat release approximately 3-5 months later. Figure 3d shows that the strong (weak) sea-to-air heat flux implies reduction (increase) of the SLP over the same region, with a lag of 3-5 months. This illustrates how the pressure field is responding to the

changes in the underlying sea ice extent.

A similar SLP change occurs in the Bellingshausen Sea approximately 6-12 months before it takes place in the Weddell Sea (snapshots 6-7 and 2-3), owing to the same process occurring over the SIC anomaly there (Venegas et al., submitted manuscript, 2001). As such, the SLP change is seen as a propagating pattern coming from the west, that appears to be sustained owing to the regulating impact of ice on the ocean-atmosphere heat fluxes. The resulting change in the atmospheric pattern over the Weddell Sea initiates a new sequence of air-ice-sea interactions similar to those described in sections 4.1 and 4.2 but of opposite sign. This gives rise to self-sustained coupled oscillations in the South Atlantic sector of Antarctica, which seem to be closely related to similar-scale coupled variations in the South Pacific sector (Venegas et al., submitted manuscript, 2001).

4.4. Extreme Situations

Figure 4 shows the complete SLP and ID fields (climatologies plus anomalies) and the 0.15 SIC isoline for summer and winter, corresponding to the two extreme situations of snapshots 1 and 5. The isobar configurations in the two extreme cases illustrate the intensity changes in the zonal SLP gradient and hence in the meridional geostrophic winds to the east of the Antarctic Peninsula. The ID patterns reveal the differences in the direction and speed of the sea ice motion in the zonal and meridional branches of the gyre. Meridional ID velocities in the northward branch of the gyre are 33% smaller in 1 than in 5. Zonal ID velocities in the East Wind Drift are 20% larger in 1 than in 5. The combination of large ice import from the east and weak ice export to the north in 1 results in accumulation and replenishment of ice in the inner Weddell Sea (positive CL anomaly). The opposite situation occurs in 5. The summer 0.15 SIC isoline shows how the summer ice edge extends to the east (1) or retreats (5) in the southeastern Weddell Sea (Coats Land region). The winter 0.15 SIC isoline illustrates the effect of the SO anomaly on the northward ice extent.

5. The Long-Term Trend

Plates 3a and 3b show the reconstructed SIC, SLP, and ID anomalies at the point of maximum amplitude of the long-term signal. As stated earlier, the period of oscillation of this low-frequency signal is not well defined (owing to the shortness of the available data set) and it is ambiguous whether this is a long-term trend or a decadal-scale oscillation. Recent works by *Thompson et al.* [2000], *Simmonds and Keay* [2000], and *Watkins and Simmonds* [2000] provide evidence for a truly long-term trend in this region during the recent years, which further supports the validity of this low-

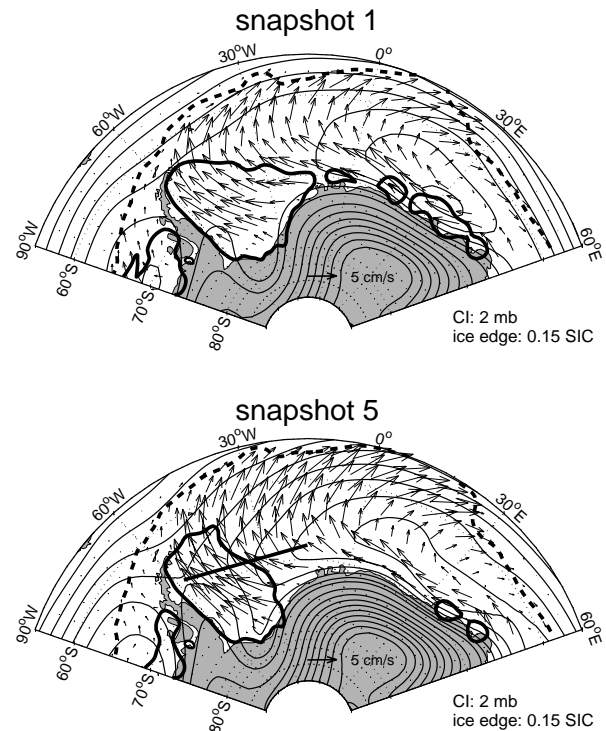


Figure 4. The two extreme situations of the quasi-quadrennial oscillation corresponding to snapshots 1 and 5 of Plates 1 and 2. The SLP and ID patterns are constructed as the sum of the climatologies (Figures 1c and 1d, respectively) and the anomalous patterns of snapshots 1 and 5. The summer (solid lines) and winter (dashed lines) 0.15 SIC isolines are drawn to illustrate the extent of the ice margin in each situation. The straight line shows the definition of the zonal SLP gradient described in the text. The ID field is shown for the case of maximum (winter) ice extent.

frequency signal detected by the MTM-SVD method.

The SIC spatial pattern (Plate 3a) shows a monopole structure with a large anomaly situated in the Central Weddell, around 30°W-70°S. The time evolution of the “Central Weddell SIC anomaly” is shown in Plate 3c and indicates that the SIC anomaly reaches a maximum around 1994 (positive phase of the trend shown in Plate 3a), and a minimum around 1987. Besides the Central Weddell SIC anomaly, two weaker centers of action of the opposite sign appear along the east coast of the Antarctic Peninsula and in the region of Maud Rise, near 5°E-63°S. The latter is especially interesting, since it coincides with the typical loca-

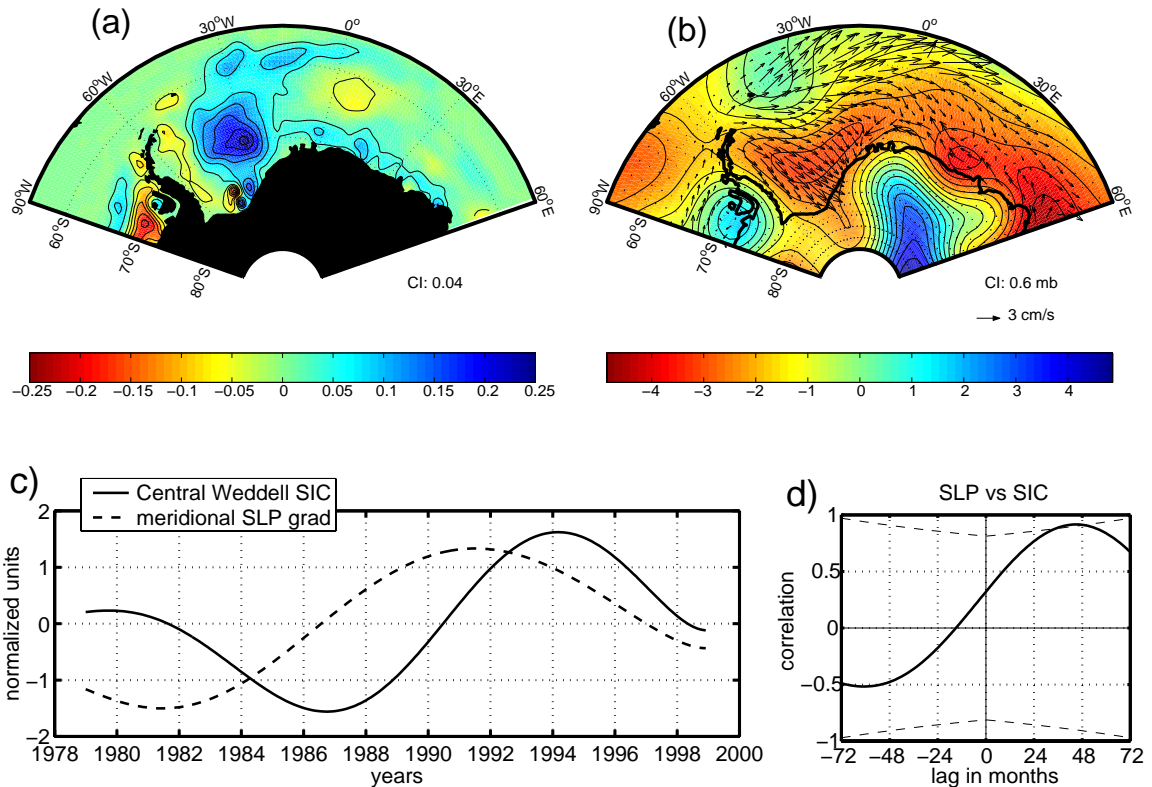


Plate 3. Spatial reconstruction of the (a) SIC anomalies and (b) SLP and ID anomalies at the point of maximum amplitude of the long-term signal (around 1994). The negative phase (around 1987) corresponds to the opposite-signed patterns (not shown). Zero contour is omitted in the SIC patterns. The ID patterns are shown for the case of maximum (winter) sea ice extent. (c) Temporal evolution of the Central Weddell SIC anomaly and of the meridional SLP gradient defined as the pressure at 40°W-57°S minus that at 40°W-73°S (see straight line in Figure 5). Time series are low passed with a cutoff period of 10 years and normalized by the standard deviation. (d) Lagged correlation function between the two time series on the left, with 90% significance levels (dashed lines). The meridional SLP gradient leads the Central Weddell SIC by 3-4 years, but the correlation is barely significant owing to the shortness of the record.

tion of the winter Weddell polynya. The presence of a negative SIC anomaly in the region of Maud Rise in Plate 3a is consistent with the opening of a transient polynya in the winter of 1994 [Drinkwater, 1996]. An earlier and more dramatic appearance of the winter Weddell polynya in 1974-1976 [Carsey, 1980; Comiso and Gordon, 1987; Gordon and Comiso, 1988; Parkinson, 1992] may suggest an oscillatory behavior in the occurrence of the Weddell polynya and in the long-term signal discussed here.

The main feature in the SLP pattern (Plate 3b) is a center of action in the southern Weddell Sea, accompanied by another of opposite sign to the north, near 40°W - 60°S . Consistently, ID anomalies present a strong zonal component in a broad region along 60°S , which reinforces the climatological eastward branch of the Weddell Gyre. An elongated zone of ice divergence is also observed along 63°S , from the tip of the Antarctic Peninsula to the Maud Rise region. Much of the momentum transferred via wind stress to the ice is further transferred via ice-ocean stress to the upper ocean. The vorticity associated with the ice divergence causes Ekman pumping, doming of the pycnocline, and entrainment of warm deep water. This warm deep water is particularly close to the surface near Maud Rise, where the pycnocline depth reaches a minimum [Martinson and Iannuzzi, 1998]. Warm water entrainment during storm events may therefore be strong enough to significantly reduce the ice concentration by melting ice in the vicinity of Maud Rise, and thus be responsible for the opening of the transient Weddell polynya event in 1994.

Figure 5 shows the complete SLP and ID fields during the extreme phases of the long-term signal, that is, around 1987 and 1994, and the position of the summer and winter ice edge as in Figure 4. The SLP pattern in the year 1994 shows a squeezed and zonally elongated low-pressure center that reaches the Weddell Sea interior from the east, implying an intensified Circumpolar Trough. The ID field reflects this fact by showing a well-defined Weddell Gyre with strong eastward and westward branches. A zone of strong compression and shear occurs in the central Weddell Sea (around 30°W - 70°S) where the westward drift piles up against the peninsula. This ice convergence is reflected by the extended summer ice covered area in 1994 (positive Central Weddell SIC anomaly). In contrast, the SLP pattern in 1987 shows a broad low-pressure center with a large meridional extent and, consequently, anomalously strong meridional winds over the entire Weddell basin. The corresponding ID field shows a clearly deformed Weddell Gyre, with almost no zonal motion and predominantly northward ice drift. This results in ice divergence from the Weddell basin and is reflected by the retreated summer ice covered area in 1987 (negative Central Weddell SIC anomaly).

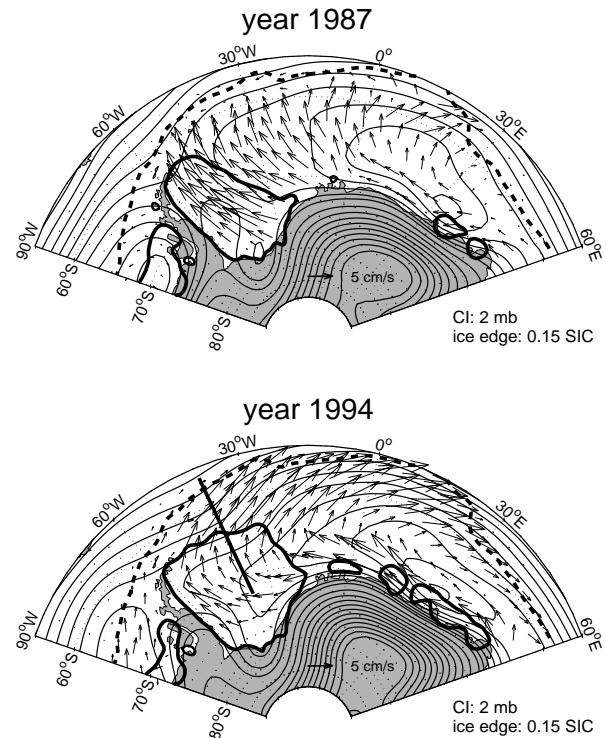


Figure 5. The two extreme situations of the long-term signal corresponding approximately to years 1987 and 1994. The SLP and ID patterns are constructed as the sum of the climatologies (Figures 1c and 1d, respectively) and the anomalous pattern of Plate 3b (for 1994) and its opposite-signed counterpart (for 1987). The summer (solid lines) and winter (dashed lines) 0.15 SIC isolines are drawn to illustrate the extent of the ice margin in each situation. The straight line shows the definition of the meridional SLP gradient described in the text. The ID field is shown for the case of maximum (winter) ice extent.

The atmospheric forcing of the Central Weddell SIC anomaly is also illustrated in Plates 3c and 3d. The temporal evolution of the meridional SLP gradient (SLP difference across the straight line in Figure 5) also shows a positive trend that leads the Central Weddell SIC fluctuation by approximately 3-4 years. The change in the Weddell Gyre circulation near 1990 appears to have been preceded by an atmospheric circulation change a few years earlier and is recorded in large-scale sea ice drift data [Drinkwater *et al.*, 1999a]. Similar changes in the ice and atmospheric circulation regimes around 1990 have also been reported by Jacobs and Comiso [1997] in the Bellingshausen Sea and by

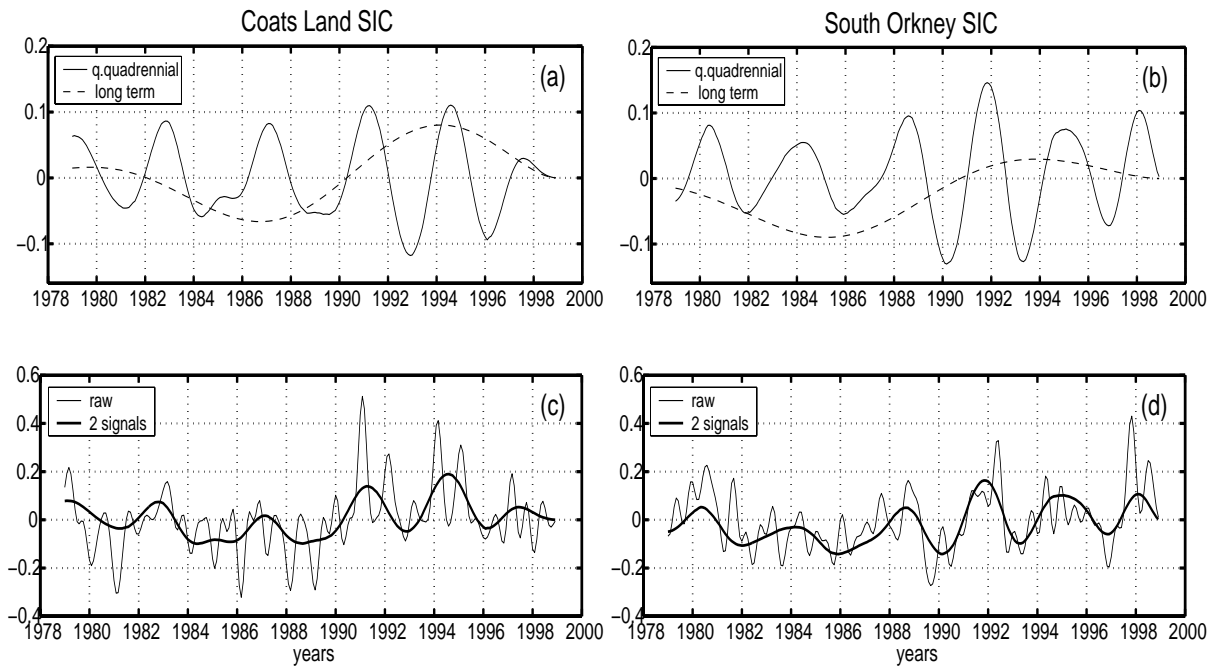


Figure 6. (top) Quasi-quadrennial signal and long-term trend in SIC in (a) the Coats Land region (45° - 15° W and 65° - 77° S) and (b) the South Orkney region (60° - 15° W and 55° - 65° S). (bottom) Sum of the two signals (thick line) and raw monthly SIC anomalies (thin line) in (c) the Coats Land region and (d) the South Orkney region. Units are fraction of the area covered by ice.

Cullather et al. [1996] and *Bromwich et al.* [2000] in the Ross-Amundsen Seas. The coupling with the slow adjusting ocean may account for the long-timescale character of this signal.

Icebergs grounded since the late 1980s to the north of Berkner Island (at 45° W- 77° S) between the Ronne and Filchner Ice Shelves [*Zibordi and Van Woert*, 1993] have prevented significant inflow of sea ice into the southern Weddell Sea over the last decade or so. These grounded icebergs represent a disturbance to the flow along the Coats Land coast in contrast to the smooth coastal inflow in the traditional cyclonic gyre circulation. This results in pile up of ice in the central Weddell during the last decade and may also be linked to the change in circulation regime that occurred after 1990.

6. Sea Ice Temporal Variability

The interplay of the two described signals is illustrated in Figure 6 by the temporal evolution of the quasi-quadrennial and long-term SIC variations, and that of their sum, in the

CL and SO regions. Both signals are comparable in amplitude in the CL region, but the quasi-quadrennial signal is slightly dominant in the SO region. Peak values are observed during summer-fall in the CL raw anomalies and during winter-spring in the SO raw anomalies, which is consistent with the seasonal character of the anomalies discussed earlier. The total signal (that is, the sum of the quasi-quadrennial and long-term modes) accounts for 35% and 45% of the variance of the monthly sea ice fluctuations in the CL and SO regions, respectively. This percentage increases substantially, however, when considering only the relevant season for each region: the CL signal accounts for 73% of the summer (January-March) ice variance, while the SO signal accounts for 57% of the winter (July-September) ice variance.

In the CL region, the quasi-quadrennial and long-term signals add constructively around 1991 and 1994 (Figure 6a), which results in years of largest ice extent in the 20-year record (Figure 6c) [*Cavaliere et al.*, 1997b]. In contrast, in 1987 and 1993 the two signals are clearly out of phase and their effects cancel each other, which results in almost zero

ice anomalies.

In the SO region, however, the long-term mode is not strong enough to disturb the quasi-quadrennial cycles, which are well defined during the 20 years. *Harms et al.* [2001] have observed minimum and maximum net ice mass flux from the Weddell Sea in 1990 and 1991, respectively, which is consistent with the largest peaks of the quasi-quadrennial signal in the SO region (Figure 6b). Furthermore, *Drinkwater et al.* [1999a] identify 1990 as the most sluggish northward ice drift during the satellite era. In contrast, 1991 was identified from upward looking sonar and satellite ice drift data to have the largest winter peak in net northward ice area flux [*Drinkwater et al.*, 2001].

The quasi-quadrennial signal alone accounts for 25% and 40% of the monthly ice concentration variance in the CL and the SO regions, respectively. Frequency and amplitude modulations are evident in both regions, the oscillations being of smaller amplitude and of relatively longer period (~ 4 years) up to about 1988/1990 and of larger amplitude and shorter period (~ 3 years) afterward. *Gloersen* [1995] identified a distinct period of oscillation of 4 years in the Weddell sea ice extent during the 9-year period 1978-1987, which coincides with our pre-1988 period. The quasi-quadrennial SIC cycles are particularly well defined from 1988/1990 onward. Furthermore, the lead-lag relationships among the time series shown in Figure 3 are also more clear after 1988/1990. This may suggest that the change in regime in the Weddell atmospheric and oceanic circulation around 1990 discussed in section 5 interferes with the quasi-quadrennial cycles, partly accounting for the different character of the time series before and after 1990.

The long-term trend alone accounts for 20% and 8% of the monthly ice extent variance in the CL and the SO regions, respectively. Its relative importance in the CL region reflects the strong summer signature of this signal.

7. Discussion and Conclusions

Sea ice variability in the Weddell Sea is dominated by quasi-quadrennial (3- to 4-year period) oscillations and is strongly coupled to atmospheric and oceanic fluctuations. The sea ice, the upper ocean, and the atmosphere alternatively force one another, leading to air-ice-sea interactions and feedbacks that account for the oscillating behavior of the system.

Anomalous atmospheric configurations periodically generate sea ice concentration anomalies of alternating sign in the southeastern Weddell Sea. These are swept out of the basin the following year and advected eastward by the gyre circulation. The eastward propagation of ice anomalies along the winter ice edge accounts for the passage of

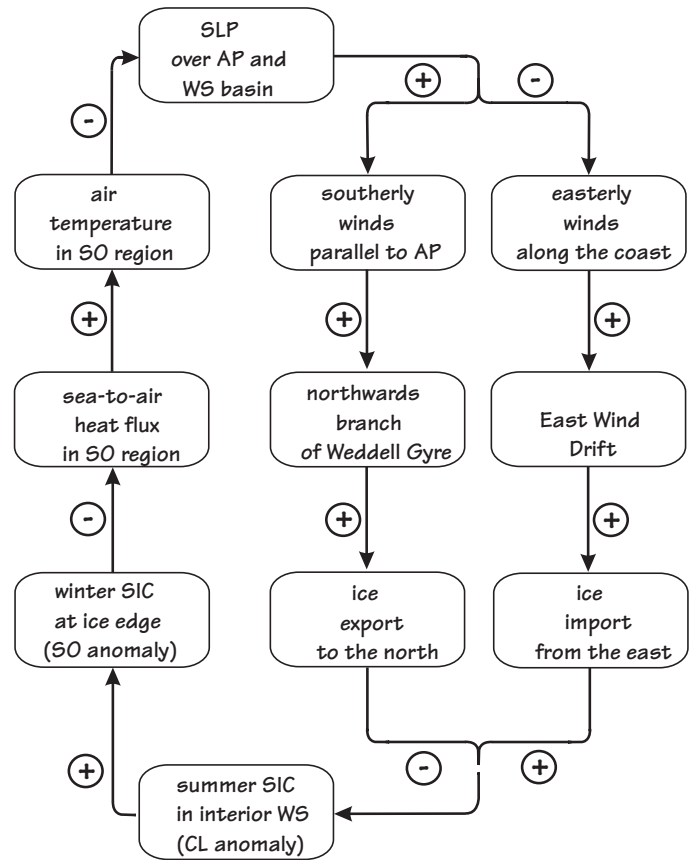


Figure 7. Schematic representation of the sequence of processes involved in one half of a quasi-quadrennial Weddell Sea Oscillation. A positive sign between two boxes indicates that a positive (negative) anomaly in the first quantity leads to a positive (negative) anomaly in the second. A negative sign between two boxes indicates that a positive (negative) anomaly in the first quantity leads to a negative (positive) anomaly in the second [*Kellogg*, 1983]. AP, Antarctic Peninsula, WS, Weddell Sea.

the ACW through the Atlantic sector of the Southern Ocean. This variability in ice dynamics forces changes in northward ice extent. These result in strong fluctuations in heat release from the ocean to the atmosphere in the region close to the ice edge, which in turn causes changes in the atmospheric pressure. A suitable combination of these processes results in a coupled air-ice-sea “Weddell Sea Oscillation.”

The feedback loop of Figure 7 illustrates schematically the sequence of interactions involved in one half of a quasi-quadrennial cycle. The interpretation of the signs and arrows in the loop follows that described by *Kellogg* [1983]

and *Mysak and Venegas* [1998]. A perturbation that is transferred from one box to the next (in the clockwise direction) returns to its initial box with opposite sign; that is, Figure 7 represents one half of a climate cycle. The period of the oscillation is the time taken to traverse the loop twice. The “oscillation” works as follows. Reduced SLP over the Antarctic Peninsula and the Weddell basin (snapshot 1 of Plate 1) leads to northeasterly wind anomalies over the entire Weddell basin. Such anomalies weaken the southerly winds parallel to the Antarctic Peninsula and enhance the easterly winds parallel to the coast. These anomalous winds drive a weak northward branch and a strong westward branch of the Weddell Gyre. This results in weak ice export from the interior Weddell Sea to the north and strong ice import to the interior Weddell Sea from the east. Consequently, sea ice accumulates in the interior Weddell Sea, as reflected by an increased summer ice concentration (positive Coats Land SIC anomaly). Northward sea ice advection by the mean gyre circulation results in increased northward ice extent the following winter (positive South Orkney SIC anomaly). The reduced open water area along the winter ice margin in the South Orkney region implies a reduction in sea-to-air heat flux, a cooling of the lower troposphere and an increase in SLP over the South Orkney region. This combines with the positive SLP anomaly coming from the Bellingshausen Sea to yield increased SLP over the Antarctic Peninsula and the Weddell basin (snapshot 5 of Plate 2), thereby completing the loop. A similar sequence of reversed-signed processes traverses the loop to complete the second half of a quasi-quadrennial oscillation.

Results from our ongoing research (Venegas et al., submitted manuscript, 2001) suggest that similar coupled mechanisms also occur in other sectors of Antarctica, particularly in the Ross, Amundsen, and Bellingshausen Seas. This would indicate that the passage of the ACW around Antarctica is strongly linked to regional air-ice-sea coupling processes that are phase shifted among the different basins. This hypothesis, however, does not exclude the possibility of external forcings to the ACW, such as SLP and sea surface temperature anomalies arriving from the tropical western South Pacific and related to El Niño-Southern Oscillation (ENSO) [Peterson and White, 1998]. We suggest therefore that the Weddell Sea Oscillation may have a life of its own inside the basin and, at the same time, may be properly synchronized with such remote ENSO forcing that determines its inter-annual timescale. As such, the regional coupling discussed here seems to be the high-latitude manifestation of large-scale atmospheric circulation anomalies which are driven via teleconnections with ENSO.

Sea ice variability on timescales longer than 10 years is also detected in the Weddell Sea, albeit rather speculatively

in this 20-year-long record. The atmospheric circulation is proposed to account for these long-term ice fluctuations by driving slow changes in the shape and characteristics of the Weddell Gyre. An intensified Circumpolar Trough leads to a zonally elongated gyre. A strong zonal (westward) component of ice flow results in high ice concentration in the central Weddell Sea through accumulation of ice against the Antarctic Peninsula. This situation dominated the last decade of the record (after 1990) when several large icebergs were grounded off the Filchner Ice Shelf, thereby disturbing the normal westward flow along the Coats Land coast. On the other hand, a meridionally extended gyre with predominantly northward motion favors low ice concentration in the central Weddell Sea, owing to exaggerated net ice export to the north. Such was the situation during the first decade of the record, up to 1990. The change in the Weddell Gyre circulation regime was preceded by a change in the general atmospheric pattern with a lag of 3-4 years. Such a delay results from the slow response of the oceanic gyre to adjust to the atmospheric changes. The integrative effect of the ocean may account for the long-timescale character of this signal.

An intriguing feature of the long-term signal is an area of depleted ice concentrations and enhanced ice divergence in the region of Maud Rise around 1994, which coincides with the appearance of a transient winter Weddell polynya. If we speculate that the long-term signal has in fact some periodic behavior on the quasi-decadal timescale, and back-project the long-term SIC fluctuation shown in Figure 6a, we might suggest that the last time when this signal was in a positive phase coincides with the time of the appearance of the 1974-1976 Weddell polynya. The requirement, however, for the likely appearance of a polynya would be the coincident positive phase of the long-term signal with a peak in Weddell Deep Water potential temperature. The latter could precondition the upper ocean over a broad area to the situation of marginal stability [Martinson and Iannuzzi, 1998] in which the right blend of air-ice-sea couplings would be required to trigger a polynya event.

Acknowledgments. The authors are grateful to Michael Mann, Gary Shaffer, Michael Williams, Detlef Quadfasel, Douglas Martinson, Ian Simmonds and Jeffrey Park for valuable comments and input. S.A.V. gratefully acknowledges the Danish National Research Foundation for its support. M.R.D. performed this work at the Jet Propulsion Laboratory, California Institute of Technology. The SMMR and SSM/I sea ice concentration data have been obtained from the EOS Distributed Active Archive Center at the National Snow and Ice Data Center, University of Colorado, Boulder. The ice drift data were produced by the Polar Remote Sensing Group at the Jet Propulsion Laboratory, California Institute of Technology. Sea level pressure and heat flux data were obtained from the 40-year NCEP/NCAR Reanalysis Project.

References

- Agnew, T., H. Le, and T. Hirose, Estimation of large-scale sea-ice motion from SSM/I 85.5 GHz imagery, *Ann. Glaciol.*, 25, 305–311, 1997.
- Banke, E. G., S. D. Smith, and R. J. Anderson, Drag coefficients at AIDJEX from sonic anemometer measurements, in *Sea Ice Processes and Models: Arctic Ice and Dynamics Joint Experiment (AIDJEX) International Commission on Snow and Ice Symposium*, edited by R. S. Pritchard, pp. 430–442, Univ. of Wash. Press, Seattle, 1980.
- Bromwich, D. H., A. N. Rogers, P. Kållberg, R. I. Cullather, J. W. C. White, and K. J. Kreutz, ECMWF analyses and re-analyses depiction of ENSO signal in Antarctic precipitation, *J. Clim.*, 13, 1406–1420, 2000.
- Carsey, F., Microwave observations of the Weddell Polynya, *Mon. Weather Rev.*, 108, 2032–2044, 1980.
- Cavalieri, D. J., C. L. Parkinson, P. Gloersen, and H. J. Zwally, Arctic and Antarctic sea ice concentrations from multichannel passive-microwave satellite data sets: Oct. 1978 to Sep. 1995, *NASA Tech. Rep. #104627*, 17 pp., 1997a.
- Cavalieri, D. J., P. Gloersen, C. L. Parkinson, J. C. Comiso, and H. J. Zwally, Observed hemispheric asymmetry in global sea ice changes, *Science*, 278, 1104–1106, 1997b.
- Cavalieri, D. J., C. L. Parkinson, P. Gloersen, J. C. Comiso, and H. J. Zwally, Deriving long-term time series of sea ice cover from satellite passive-microwave multisensor data sets, *J. Geophys. Res.*, 104, 15,803–15,814, 1999.
- Comiso, J. C., and A. L. Gordon, Recurring polynyas over the Cosmonaut Sea and the Maud Rise, *J. Geophys. Res.*, 92, 2819–2834, 1987.
- Comiso, J. C., and A. L. Gordon, The Cosmonaut Polynya in the Southern Ocean: Structure and variability, *J. Geophys. Res.*, 101, 18,297–18,313, 1996.
- Comiso, J. C., and A. L. Gordon, Interannual variability in summer sea-ice minimum, coastal polynyas and bottom water formation in the Weddell Sea, in *Antarctic Sea Ice: Physical Processes, Interactions and Variability*, *Antarct. Res. Ser.*, vol. 74, edited by M. O. Jeffries, pp. 293–315, AGU, Washington, D. C., 1998.
- Cullather, R. I., D. H. Bromwich, and M. L. Van Woert, Interannual variations in Antarctic precipitation related to El Niño-Southern Oscillation, *J. Geophys. Res.*, 101, 19,109–19,118, 1996.
- Deacon, G., *The Antarctic Circumpolar Ocean*, 180 pp., Cambridge Univ. Press, New York, 1984.
- Dierking, W., Laser profiling of the ice surface topography during the Winter Weddell Gyre Study 1992, *J. Geophys. Res.*, 100, 4807–4820, 1995.
- Drinkwater, M. R., Satellite microwave radar observations of climate-related sea ice anomalies, in *Workshop on Polar Processes and Climate Change*, pp. 115–119, Am. Meteorol. Soc., Boston, Mass., 1996.
- Drinkwater, M. R., Satellite microwave radar observations of Antarctic sea ice, in *Analysis of SAR Data of the Polar Ocean*, edited by C. Tsatsoulis and R. Kwok, pp. 145–187, Springer-Verlag, New York, 1998a.
- Drinkwater, M. R., Active microwave remote sensing observations of Weddell Sea ice, in *Antarctic Sea Ice: Physical Processes, Interactions and Variability*, *Antarct. Res. Ser.*, vol. 74, edited by M. O. Jeffries, pp. 187–212, AGU, Washington, D. C., 1998b.
- Drinkwater, M. R., R. Kwok, C. A. Geiger, J. A. Maslanik, C. W. Fowler, and W. J. Emery, Quantifying surface fluxes in the ice-covered polar oceans using satellite microwave remote sensing data, in *Proceedings of OCEANOBS'99: The Ocean Observing System for Climate*, vol. 1, Cent. Nat. Etudes Spatiales, Saint Raphael, France, 1999a.
- Drinkwater, M. R., X. Liu, J. Maslanik, and C. Fowler, Optimal analysis products combining buoy trajectories and satellite-derived ice-drift field, in *International Programme for Antarctic Buoy, IPAB Biennial Meeting Report, May 11-13, 1998, Naples, Italy, WCRP Rep. 5/1999*, pp. 1-11, World Clim. Res. Program, Geneva, Switzerland, 1999b.
- Drinkwater, M. R., X. Liu, and S. Harms, Combined satellite- and ULS-derived sea-ice flux in the Weddell Sea, *Ann. Glaciol.*, 33, in press, 2001.
- Efron, B., *The Jackknife, the Bootstrap and Other Resampling Plans*, 92 pp., Soc. for Appl. and Ind. Math., Philadelphia, Pa., 1990.
- Emery, W. J., C. W. Fowler, and J. A. Maslanik, Satellite-derived maps of Arctic and Antarctic sea ice motion: 1988-1994, *Geophys. Res. Lett.*, 24, 897–900, 1997.
- Fahrbach, E., G. Rohardt, N. Scheele, M. Schröder, V. Strass, and A. Wisotzki, Formation and discharge of deep and bottom water in the northwestern Weddell Sea, *J. Mar. Res.*, 53, 515–538, 1995.
- Fisher, R., and V. I. Lytle, Atmospheric drag coefficients of Weddell Sea ice computed from roughness profiles, *Ann. Glaciol.*, 27, 455–460, 1998.
- Gloersen, P., Modulation of hemispheric sea ice cover by ENSO events, *Nature*, 373, 503–506, 1995.
- Gordon, A. L., and J. C. Comiso, Polynyas in the Southern Ocean, *Sci. Am.*, 256, 90–97, 1988.
- Gordon, A. L., and B. A. Huber, Southern Ocean winter mixed layer, *J. Geophys. Res.*, 95, 11,655–11,672, 1990.
- Gordon, A. L., B. A. Huber, H. H. Hellmer, and A. Ffield, Deep and bottom water of the Weddell Sea's western rim, *Science*, 262, 95–97, 1993.
- Harangozo, S. A., Atmospheric meridional circulation impacts on contrasting winter sea-ice extent in two years in the Pacific sector of the Southern Ocean, *Tellus, Ser. A*, 49, 388–400, 1997.
- Harms, S., E. Fahrbach, and V. H. Strass, Sea ice transports in the Weddell Sea, *J. Geophys. Res.*, 106, 9057–9073, 2001.
- Ivchenko, V. O., A. E. Krupitsky, V. M. Kamenkovich, and N. C. Wells, Modeling the Antarctic Circumpolar Current: A comparison of FRAM and equivalent barotropic model results, *J. Mar. Res.*, 57, 29–46, 1999.
- Jacobs, G. A., and J. L. Mitchell, Ocean circulation variations associated with the Antarctic Circumpolar Wave, *Geophys. Res. Lett.*, 23, 2947–2950, 1996.
- Jacobs, S. S., and J. C. Comiso, Sea-ice and oceanic processes on the Ross Sea continental shelf, *J. Geophys. Res.*, 94, 18,195–18,211, 1989.
- Jacobs, S. S., and J. C. Comiso, Climate variability in the Amundsen and Bellingshausen Seas, *J. Clim.*, 10, 697–709, 1997.
- Kalnay, E., et al., The NCEP/NCAR 40-year Reanalysis Project, *Bull. Am. Meteorol. Soc.*, 77, 437–471, 1996.

- Kaylor, R. E., Filtering and decimation of digital time series, *Tech. Rep. BN 850*, Univ. of Md., College Park, 1977.
- Kellogg, W. W., Feedback mechanisms in the climate system affecting future levels of carbon dioxide, *J. Geophys. Res.*, **88**, 1263–1269, 1983.
- Kottmeier, C., and D. Engelbart, Generation and atmospheric heat exchange of coastal polynyas in the Weddell Sea, *Boundary Layer Meteorol.*, **60**, 207–234, 1992.
- Kottmeier, C., and L. Sellmann, Atmospheric and oceanic forcing of Weddell Sea ice motion, *J. Geophys. Res.*, **101**, 20,809–20,824, 1996.
- Kwok, R., Recent changes in Arctic Ocean sea-ice motion associated with the North Atlantic Oscillation, *Geophys. Res. Lett.*, **27**, 775–778, 2000.
- Kwok, R., A. Schweiger, D. A. Rothrock, S. Pang, and C. Kottmeier, Sea ice motion from satellite passive microwave imagery assessed with ERS SAR and buoy motions, *J. Geophys. Res.*, **103**, 8191–8214, 1998.
- Lemke, P., The expedition Antarktis X/4 of R/V *Polarstern* in 1992, in *Reports on Polar Research*, vol. 140, 90 pp., Alfred-Wegener-Inst. for Polar and Mar. Res., Bremerhaven, Germany, 1994.
- Mann, M. E., and J. Park, Global-scale modes of surface temperature variability on interannual to century timescales, *J. Geophys. Res.*, **99**, 25,819–25,833, 1994.
- Mann, M. E., and J. Park, Joint spatiotemporal modes of surface temperature and sea level pressure variability in the Northern Hemisphere during the last century, *J. Clim.*, **9**, 2137–2162, 1996.
- Mann, M. E., and J. Park, Oscillatory spatiotemporal signal detection in climate studies: A multiple-taper spectral domain approach, *Adv. Geophys.*, **41**, 1–131, 1999.
- Markus, T., C. Kottmeier, and E. Fahrbach, Ice formation in coastal polynyas in the Weddell Sea and their impact on oceanic salinity, in *Antarctic Sea Ice: Physical Processes, Interactions and Variability*, *Antarct. Res. Ser.*, vol. 74, edited by M. O. Jeffries, pp. 273–292, AGU, Washington, D. C., 1998.
- Martin, T., and E. Augstein, Large-scale drift of Arctic sea ice retrieved from passive microwave satellite data, *J. Geophys. Res.*, **105**, 8775–8788, 2000.
- Martinson, D. G., and R. A. Iannuzzi, Antarctic ocean-ice interaction: implications from ocean bulk property distributions in the Weddell Sea, in *Antarctic Sea Ice: Physical Processes, Interactions and Variability*, *Antarct. Res. Ser.*, vol. 74, edited by M. O. Jeffries, pp. 243–271, AGU, Washington, D. C., 1998.
- Martinson, D. G., and C. Wamser, Ice drift and momentum exchange in the winter Antarctic pack ice, *J. Geophys. Res.*, **95**, 1741–1755, 1990.
- Maslanik, J., T. Agnew, M. R. Drinkwater, W. Emery, C. Fowler, R. Kwok, and A. Liu, Summary of ice-motion mapping using passive microwave data, Polar Data Adv. Group, NASA Snow and Ice Distrib. Active Arch. Cent., Nat. Snow and Ice Data Cent., *Spec. Publ.* **8**, 25 pp., Boulder, Colo., 1998.
- Maykut, G. A., Energy exchange over young sea ice in the central Arctic, *J. Geophys. Res.*, **83**, 3646–3658, 1978.
- McPhee, M. G., S. Ackley, P. Guest, B. A. Huber, D. G. Martinson, J. H. Morison, R. D. Muench, L. Padman, and T. P. Stanton, The Antarctic Zone Flux Experiment, *Bull. Am. Meteorol. Soc.*, **77**, 1221–1232, 1996.
- Mysak, L. A., and S. A. Venegas, Decadal climate oscillations in the Arctic: A new feedback loop for atmosphere-ice-ocean interactions, *Geophys. Res. Lett.*, **25**, 3607–3610, 1998.
- National Snow and Ice Data Center, Nimbus-7 SMMR Arctic and Antarctic Sea-Ice Concentration Grids and DMSP F8-F11 SSM/I Ice Concentration Grids for the Polar Regions, CD-ROM series, Boulder, Colo., 1995.
- Parkinson, C. L., Interannual variability of monthly Southern Ocean sea-ice distributions, *J. Geophys. Res.*, **97**, 5349–5363, 1992.
- Percival, D. B., and A. T. Walden, *Spectral Analysis for Physical Applications: Multitaper and Conventional Univariate Techniques*, 583 pp., Cambridge Univ. Press, New York, 1993.
- Peterson, R. G., and W. B. White, Slow oceanic teleconnections linking the Antarctic Circumpolar Wave with the tropical El Niño-Southern Oscillation, *J. Geophys. Res.*, **103**, 24,573–24,583, 1998.
- Simmonds, I., and K. Keay, Mean Southern Hemisphere extratropical cyclone behavior in the 40-year NCEP-NCAR reanalysis, *J. Clim.*, **13**, 873–885, 2000.
- Thompson, D. W. J., J. M. Wallace, and G. C. Hegerl, Annular modes in the extratropical circulation, II, Trends, *J. Clim.*, **13**, 1018–1036, 2000.
- Thomson, D. J., Spectrum estimation and harmonic analysis, *Proc. IEEE*, **70**, 1055–1096, 1982.
- Thorndike, A. S., and R. Colony, Sea ice motion in response to geostrophic winds, *J. Geophys. Res.*, **87**, 5845–5852, 1982.
- Tourre, Y. M., B. Rajagopalan, and Y. Kushnir, Dominant patterns of climate variability in the Atlantic Ocean during the last 136 years, *J. Clim.*, **12**, 2285–2299, 1999.
- Venegas, S. A., and L. A. Mysak, Is there a dominant timescale of natural climate variability in the Arctic?, *J. Clim.*, **13**, 3412–3434, 2000.
- Watkins, A. B., and I. Simmonds, Current trends in Antarctic sea-ice: The 1990s impact on a short climatology, *J. Clim.*, **13**, 4441–4451, 2000.
- White, W. B., and R. G. Peterson, An Antarctic circumpolar wave in surface pressure, wind, temperature and sea-ice extent, *Nature*, **380**, 699–702, 1996.
- Yuan, X., D. G. Martinson, and W. T. Liu, The effect of air-sea-ice interaction on winter 1996 Southern Ocean subpolar storm distribution, *J. Geophys. Res.*, **104**, 1991–2007, 1999.
- Zibordi, G., and M. L. Van Woert, Antarctic sea ice mapping using the AVHRR, *Remote Sens. Environ.*, **45**, 155–163, 1993.
- M. R. Drinkwater, European Space Agency, Oceans/Ice Unit, ESTEC Earth Sciences Division (APP-FSO), Keplerlaan 1, Postbus 299, 2200 AG Noordwijk, The Netherlands. (mark.drinkwater@esa.int)
- S. A. Venegas, Danish Center for Earth System Science, Niels Bohr Institute for Astronomy, Physics and Geophysics, University of Copenhagen, Juliane Maries Vej 30, DK-2100 Copenhagen, Denmark. (silvia@dcess.ku.dk)

Received August 16, 2000; revised April 2, 2001; accepted April 9, 2001.

This preprint was prepared with AGU's \LaTeX macros v5.01, with the extension package 'AGU++' by P. W. Daly, version 1.6 from 1999/02/24.